Earth Planet. Sci. Lett. 628 (2024) 118579

Contents lists available at ScienceDirect

Earth and Planetary Science Letters

journal homepage: www.elsevier.com/locate/epsl

Insights into magma storage depths and eruption controls at Kīlauea Volcano during explosive and effusive periods of the past 500 years based on melt and fluid inclusions

Allan H. Lerner [a,b,*], D. Matthew Sublett Jr. [c], Paul J. Wallace [a], Christina Cauley [a], Robert J. Bodnar [c]

[a] Dept. of Earth Sciences, University of Oregon, OR 97403, USA
[b] U.S. Geological Survey, Cascades Volcano Observatory, WA 98683, USA
[c] Dept. of Geosciences, Virginia Tech, VA 24061, USA

ARTICLE INFO

Keywords:
Kīlauea volcano
Melt inclusions
Fluid inclusions
Basaltic volcanism
Magmatic volatiles
Raman spectroscopy

ABSTRACT

Kīlauea Volcano experiences centuries-long cycles of explosive and effusive eruptive behavior, but the relation, if any, between these eruptive styles and changing conditions in the magma plumbing system remains poorly known. We analyze olivine-hosted melt and fluid inclusions to determine magma storage depths during the explosive-era Keanakāko'i Tephra eruptions (~1500–1840 CE) and compare these results to modern effusive-era Kīlauea eruptions (1959 Kīlauea Iki, 1960 Kapoho, 2018 lower East Rift Zone). We find that shallow (1–3 km) magma storage has persisted for centuries at Kīlauea, spanning both explosive and effusive periods. In contrast, mid-crustal zones of magma storage shallowed over time, from 5 to 8 km during the Keanakāko'i sequence to 3–5 km during the modern effusive period. Melt and fluid inclusions in high-forsterite olivine ($Fo_{86–89}$) trapped at shallow depths indicate that high-temperature magmas (1200 to ~1300 °C) commonly reach depths of ≤3 km. CO_2-rich fluid inclusions are present in olivine from all investigated Kīlauea eruptions but are larger and much more abundant in Keanakāko'i units, which we interpret as indicating that a greater volume fraction of exsolved CO_2-rich fluid was present in pre-eruptive Keanakāko'i melts. Increased amounts of CO_2-rich fluids in the Keanakāko'i-era magmas would have increased magma buoyancy and driven rapid magma ascent, thereby increasing eruption energy and enhancing near-surface magma-water interactions compared to the current effusive period.

1. Introduction

Determining the depth and location of magma storage is fundamentally important for understanding volcanic processes, interpreting geophysical and geochemical monitoring signals, and assessing hazards. At Kīlauea Volcano (Hawai'i, USA), geophysically identified magma storage regions beneath the summit include the shallow "Halema'uma'u reservoir" located 1–3 km beneath Halema'uma'u Crater, containing an estimated 1–7 km^3 of magma, and the deeper "South Caldera reservoir" at depths of 3–5 km, containing up to ~20 km^3 of magma (Poland et al., 2014; Anderson et al., 2019) (note: depths reported in this study are relative to Kīlauea's summit elevation). Petrologic studies of H_2O-CO_2 volatile saturation pressures in melt inclusions from recent Kīlauea eruptions (1959–2018 CE) indicate magma storage at depths consistent with these geophysically identified reservoirs (Anderson and Brown, 1993; Moore et al., 2015; Tuohy et al., 2016; Lerner et al., 2021a; Wieser et al., 2021).

However, volcanic plumbing systems may change temporally with variations in magma supply rate and stress state (e.g., structural collapse, faulting; Lo Forte et al., 2023). Kīlauea undergoes centuries-long periods of predominantly effusive or explosive behavior, with explosive periods following major collapses of the summit caldera (Swanson et al., 2014). Kīlauea's most recent explosive period occurred after a major caldera collapse at the end of the 'Ailā'au eruptions (1410–1470 CE) that output 4–6 km^3 of lava flows (Swanson et al., 2012). Subsequent centuries of explosive activity produced the Keanakāko'i Tephra sequence (~1500–1840 CE), which consists of up to 10-m-thick deposits of well-bedded ash, lapilli, and lithic clasts around

* Corresponding author.
E-mail address: alerner@usgs.gov (A.H. Lerner).

https://doi.org/10.1016/j.epsl.2024.118579
Received 8 October 2023; Received in revised form 28 December 2023; Accepted 10 January 2024
Available online 2 February 2024
0012-821X/Published by Elsevier B.V.

Kīlauea's summit (Swanson et al., 2012; Swanson and Houghton, 2019; note: the sequence's minimum age is after 1823 CE but before 1840 CE [D. Swanson, U.S. Geological Survey, written communication, 2022], and we consider 1840 CE as the minimum age here). Earlier explosive periods at Kīlauea produced the Uēkahuna Ash (200 BCE–1000 CE) and Pahala Ash (24–10 ka) sequences (e.g., Decker and Christiansen, 1984; Easton, 1987; Fiske et al., 2009, 2019). Erupted tephra volumes were much less during these explosive periods compared to erupted lava volumes during the modern effusive era (i.e., since ~1840 CE) (Swanson et al., 2014; Wright and Klein, 2014). Trace element patterns in olivine are consistent with decreased mantle melt fraction during the most recent (Keanakāko'i) explosive period (Mourey et al., 2022). The observations suggest that magma supply rates during explosive eras may have been notably decreased compared to effusive periods. Magmas erupted during explosive periods are commonly more primitive and contain higher proportions of high-forsterite (Fo) olivine ($Fo_{86–89}$) than magmas erupted during the modern effusive era, suggesting differences in magma storage and mixing processes during explosive and effusive eras (Helz et al., 2015; Lynn et al., 2017; Garcia et al., 2018; Mourey et al., 2022; Lynn and Swanson, 2022). For example, it is commonly assumed that eruption of primitive magma indicates deeper magma storage and rapid ascent to the surface, and this hypothesis has been invoked to explain the high-temperature magmas erupted during Kīlauea's explosive eras (Sides et al., 2014; Helz et al., 2015; Lynn et al., 2017). However, this explanation remains largely untested, as detailed geophysical and petrologic geobarometry studies are only available for

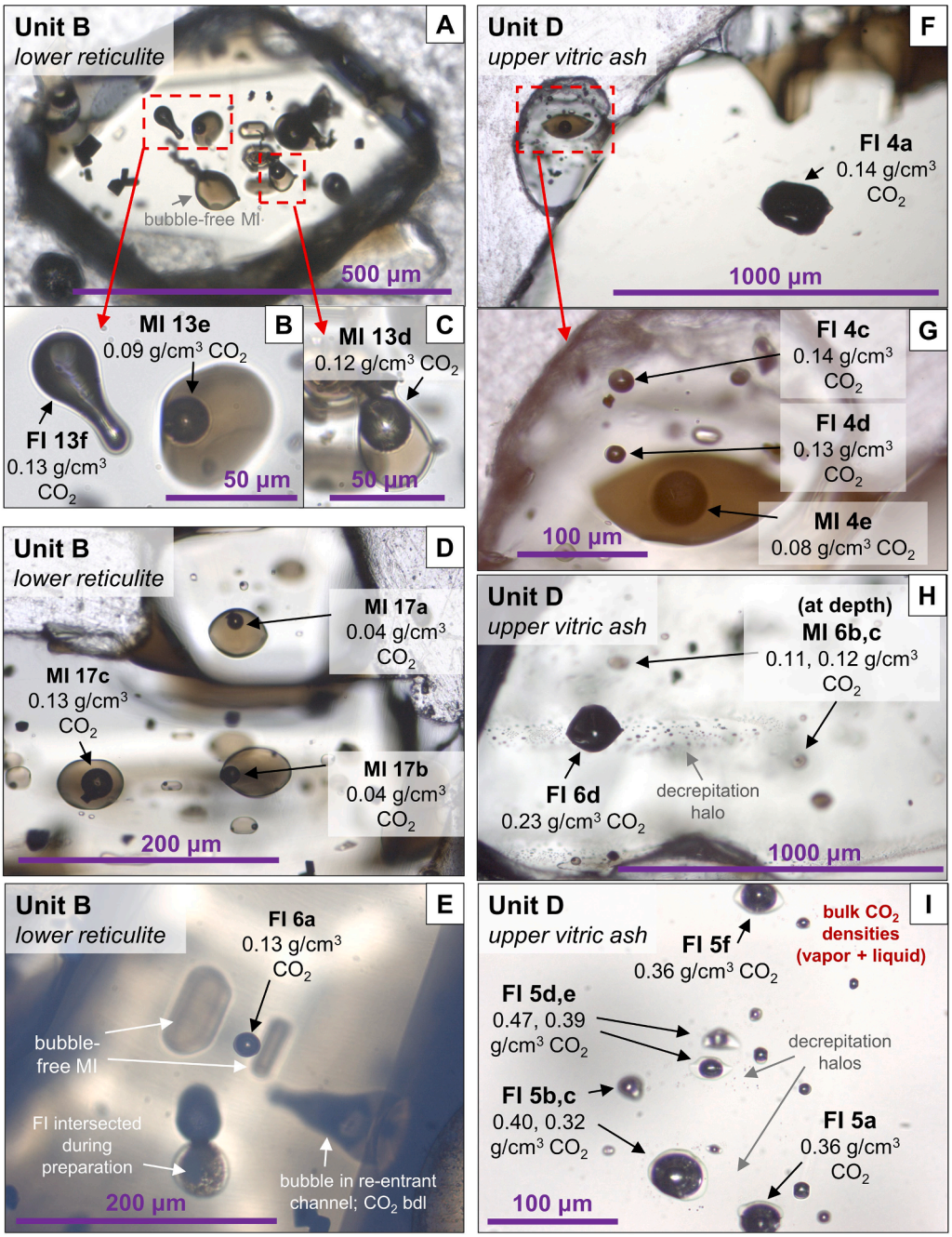

Fig. 1. Melt and fluid inclusions (FI) in olivine from the Keanakāko'i Tephra (Units B and D). Melt inclusions (MI) can be bubble-free (A,E), have small vapor bubbles (B,D), or be bubble-dominated (C,D,G). At room temperature, CO_2-rich FI exist as CO_2 vapor (A,B,E,F,G,H) ± CO_2 liquid (I). Decrepitated FI are surrounded by halos of small inclusions (H,I). Determined bulk CO_2 densities of MI vapor bubbles and FI are shown.

recent Kīlauea eruptions that involved less-primitive magmas.

The lack of robustly determined thermobarometry from Kīlauea's explosive-era eruptions limits our assessment of whether the magma plumbing configuration was vertically restructured during explosive eras. Understanding whether magma storage depths change between explosive and effusive eras is critical for improving our knowledge of the Kīlauea system (and for volcanic systems in general) and for interpreting monitoring signals that might herald a return to explosive eruptive behavior (e.g., earthquake and deformation source depths; gas compositions and emission rates). Following Kīlauea's recent caldera collapse during the 2018 lower East Rift Zone eruption (Neal et al., 2019), it became particularly prudent to study past explosive sequences to assess if, and how, the underlying magmatic system changed in response to previous caldera collapses.

Melt inclusions (MI) and fluid inclusions (FI) in phenocrysts can be used to determine pressure and temperature conditions in magmatic systems. Melt inclusions are samples of the melt phase trapped in a growing magmatic phenocryst, and fluid inclusions in magmatic systems are microsamples of exsolved fluids that are trapped within minerals during crystal growth (primary inclusions) or at some later time along healed fractures that typically form planar arrays (secondary inclusions) (e.g., Roedder, 1984). In CO_2-dominated FI, measured densities of CO_2 can be combined with equation-of-state models (e.g., Sterner and Pitzer, 1994) and estimates of magma temperature to determine entrapment pressures (e.g., Hansteen and Klügel, 2008; Dayton et al., 2023; DeVitre et al., 2023a; DeVitre and Wieser, accepted).

Here, we compare quantitative barometry of olivine-hosted FI, MI, and a third type of inclusion that is intermediate between the two – MI with a large (co-trapped) vapor bubble (Fig. 1) – to calculate entrapment pressures that reflect depths of magma crystallization and storage. We present new data from Keanakāko'i units spanning ~320 years of that eruptive sequence. These results are compared with more recent Kīlauea eruptions (1959 Kīlauea Iki, 1960 Kapoho, 2018 lower East Rift Zone) where robust barometric data are available from previous studies. Utilizing these collective datasets, we interpret the depth evolution of Kīlauea's plumbing system over the past 500 years and investigate whether variations in storage depth and exsolved fluid abundance relate to changes in eruption style. Our observations of FI also provide clear evidence for the presence of deeply exsolving CO_2-rich fluids at Kīlauea, and we propose that variations in exsolved CO_2-rich fluid fractions have played a role in influencing Kīlauea's explosive and effusive eruptive styles.

2. Melt and fluid inclusion analysis

In Kīlauea's H_2O-poor tholeiitic basaltic magma, CO_2 is the dominant component in exsolving fluids at depths >1 km (Dixon et al., 1995; Iacono-Marziano et al., 2012). Vapor bubbles in MI can contain up to 90% of the CO_2 that was dissolved in the melt at the time of trapping, so vapor bubble CO_2 must be quantified for meaningful barometric results (Steele-MacInnis et al., 2011; Hartley et al., 2014; Moore et al., 2015; Wallace et al., 2015; Hanyu et al., 2020; Wieser et al., 2021).

At Kīlauea, inclusion barometry has been constrained by quantifying CO_2 densities using Raman spectroscopy in vapor bubbles in MI (Moore et al., 2015; Lerner et al., 2021a; Wieser et al., 2021, 2022) and FI (DeVitre and Wieser, accepted), by experimentally rehomogenizing MI (Tuohy et al., 2016), and by analyzing bubble-free MI (Anderson and Brown, 1993; Lerner et al., 2021a; Wieser et al., 2021, 2022). Other studies of volatiles in Kīlauea MI have incomplete CO_2 data and, therefore, provide unreliable pressure estimates, and are excluded from our discussions here (explanations in Supplementary Materials). The studies with MI barometry based on complete CO_2 budgets have focused on olivine-hosted MI from the 1959 Kīlauea Iki eruption and the 1960 Kapoho lower East Rift Zone eruption (Anderson and Brown, 1993; Moore et al., 2015; Tuohy et al., 2016), and on olivine-, pyroxene-, and feldspar-hosted inclusions from the 2018 lower East Rift Zone eruption (Lerner et al., 2021a; Wieser et al., 2021; DeVitre and Wieser, accepted). These studies have generally investigated high-Fo olivine, and in the case of the 2018 lower East Rift Zone eruption, a mix of samples from the summit and rift zones. Collectively, these studies provide a valuable, though incomplete, barometric view into Kīlauea's magma plumbing system during select eruptions of the modern effusive era.

To extend our knowledge of magma storage barometry at Kīlauea further back in time, we present new vapor bubble and glass analyses of MI and FI from six units spanning the Keanakāko'i Tephra sequence (Supplementary Figure S1). Using the stratigraphic nomenclature and eruption ages from Swanson and Houghton (2019) and Swanson et al. (2012), these units are: Unit B lower reticulite (~1500 CE); two vitric ash samples from the lower and upper stratigraphy of Unit D (respectively, layers IIA1 and IIA2 of McPhie et al. [1990]; ~1500–1650 CE); Unit E scoria lapilli (~1650 CE); Unit J1 vitric tephra within a lithic-rich deposit related to a large block and ash surge (1790 CE); and the Unit K1 "golden pumice" (1790–1820 CE). The Unit D vitric ashes and Unit J1 lithic-rich deposits have been described as hydromagmatic sequences, whereas Units B, E, and K1 are "dry" magmatic eruptions that do not show evidence of interaction with external water (McPhie et al., 1990; Mastin et al., 2004; Swanson and Houghton, 2019; Schmith and Swanson, 2023). Olivine and MI from all samples were analyzed by electron microprobe (EPMA), and H_2O and CO_2 in MI glasses were analyzed by Fourier transform infrared spectroscopy (FTIR). Fluid inclusions and vapor bubbles in MI from the lowermost three Keanakāko'i samples (Unit B, lower- and upper-Unit D) were analyzed by Raman spectroscopy to determine CO_2 densities.

3. Results

The large majority of FI we observe in Keanakāko'i olivine do not occur along obvious healed fractures and are distributed in 3-D arrays and commonly co-mingled with MI, indicating entrapment during crystal growth (Roedder, 1984). We refer to FI occurring in this manner as primary FI. The preponderance of primary FI within the Keanakāko'i contrasts with FI observed at a number of other basaltic shield volcanoes, where the majority of FI are of secondary origin (Bureau et al., 1998; Lo Forte et al., 2023; Dayton et al., 2023). Within Keanakāko'i FI, CO_2 was the only molecular species identified by Raman analysis, consistent with expectations of CO_2 being the dominant volatile exsolving at depth from low-H_2O Kīlauea magmas (Gerlach, 1986; Dixon et al., 1995; Lerner et al., 2021a). Calculated pressures from FI and bubbles in bubble-dominated MI assume they contain pure CO_2, but if small amounts of H_2O (<10 mol%) were present the pressures could be up to 10% higher (Fig. S6). No carbonate minerals were observed on the walls of MI vapor bubbles or FI, or detected in Raman spectra. Small Fe-sulfide condensates were present at the vapor bubble/glass interface in some MI (Figure S8), similar to those identified in other Kīlauea MI (Wieser et al., 2020), but these do not affect H_2O-CO_2 barometry calculations. Full sample information, analytical methods, and thermobarometry calculations and assumptions are described in the **Supplementary Materials**.

Olivine crystals in the Keanakāko'i eruptive units that we analyzed are generally Mg-rich ($Fo_{82–89}$), with calculated crystallization temperatures of 1170–1300 °C (from MgO-thermometry [Helz and Thornber, 1987] of post-entrapment crystallization-corrected [Danyushevsky and Plechov, 2011] MI) (**Figure S11**). These results are similar to previous studies of Keanakāko'i olivine that also identified a predominance of high-Fo compositions (e.g., Sides et al., 2014; Lynn et al., 2017; Mourey et al., 2022). Interestingly, we found only lower-Fo olivine ($Fo_{82–84}$) in the Unit B reticulite, whereas high-Fo grains (up to Fo_{89}) have been reported for Unit B in other studies (Sides et al., 2014; Lynn et al., 2017; Mourey et al., 2022), perhaps indicating that we analyzed a specific sub-unit within this unit.

Olivine-hosted MI that we analyzed in the Keanakāko'i units generally contain 0.4–0.6 wt% H_2O and 1100–1500 ppm S, similar to

concentrations measured in many modern, effusive-era Kīlauea eruptions (Anderson and Brown, 1993; Sides et al., 2014; Tuohy et al., 2016), but elevated compared to the relatively H_2O- and S-poor MI present in the 2018 lower East Rift Zone eruption (Lerner et al., 2021a) (Figs. 2, 3). Sulfur concentrations in Keanakāko'i MI increase as glass MgO decreases from 14 to 10 wt%, then remain relatively invariant at 1250–1450 ppm from ~10 to 7 wt% MgO. This suggests initial sulfur enrichment as an incompatible element until sulfide saturation is reached during further magma cooling and fractional crystallization, and is consistent with sulfide saturation models for Kīlauea magmas when 20–30% of total molar sulfur in the melt is present as S^{6+} (Wieser et al., 2020; Lerner et al., 2021a, 2021b).

Dissolved H_2O concentrations in Keanakāko'i MI slightly decrease with decreasing glass MgO, suggesting H_2O may not follow incompatible element behavior. However, interpreting the record of H_2O in olivine-hosted MI is complicated due to rapid diffusive equilibration of H_2O through olivine crystals (e.g., Portnyagin et al., 2008). Deciphering the competing effects of incompatible element enrichment, volatile degassing, mixing of variably degassed magmas, and diffusive equilibration in controlling H_2O concentrations in Keanakāko'i MI is beyond the scope of this manuscript. At these low H_2O concentrations, small variations caused by post-entrapment diffusive hydrogen loss has a trivial effect on calculated vapor saturation pressures.

Total CO_2 concentrations (glass + vapor bubble) in Keanakāko'i MI range widely (200–2000 ppm CO_2) in high-MgO glasses and become restricted to lower concentrations (≤500 ppm, rarely to 800 ppm) in glasses with MgO <9 wt% (Figs. 2, 3); the implications of these CO_2 observations are discussed in detail below.

Glass preserved within melt embayments in olivine, as interstitial glass between crystals, and as matrix glass adhering to crystals contains 7–10 wt% MgO, and MgO-thermometry (Helz and Thornber, 1987) indicates erupting magma temperatures of 1150–1210 °C across the Keanakāko'i sequence. Melt embayments and interstitial glasses, which are partially isolated from degassing, contain 0.1–0.5 wt% H_2O, 140–1400 ppm S, and ≤200 ppm CO_2. Matrix glasses have lower volatile concentrations of 0.1–0.3 wt% H_2O, 100–900 ppm S, and undetectable CO_2 (<50 ppm), indicating partial degassing of H_2O and S, and near-complete degassing of CO_2 during ascent and quenching (Fig. 3). Vitric ash samples from the Unit D phreatomagmatic tephra have the highest residual matrix glass H_2O and S concentrations (Fig. S2), consistent with incomplete volatile degassing due to rapid quenching, presumably during interaction with external water (Mastin et al., 2004; Schmith and Swanson, 2023).

3.1. Treatment of melt inclusions with large, co-trapped vapor bubbles

Inclusions in Keanakāko'i olivine contain a wide range of bubble proportions, from bubble-free MI (100% glass) to isolated FI (no observable glass) (Fig. 1). A single, small-bubble occupying <~8 vol% in an MI is usually interpreted to have formed during post-entrapment processes, whereas a larger bubble (>10 vol% of the MI) likely results from the co-entrapment of melt and an exsolved fluid phase (i.e., heterogenous entrapment) (Frezzotti, 2001; Lowenstern, 2003; Moore et al., 2015; Aster et al., 2016; Hanyu et al., 2020). We refer to the former as "normal" MI and the latter as "bubble-dominated" MI. Our measurements of Keanakāko'i samples confirm these interpretations, as CO_2 densities in FI and bubble-dominated MI vapor bubbles are systematically higher (0.11–0.47 g/cm^3 [n = 61]) than CO_2 densities in "normal" small-volume MI bubbles (0.02–0.12 g/cm^3 [n = 23]) (Fig. 4). If the large bubbles had formed post-entrapment from CO_2 exsolution within MI, and if we reconstruct the original melt composition based on bubble size and CO_2 densities, up to several wt% CO_2 would have been dissolved in the initial melt; these elevated CO_2 concentrations are unreasonably high for Kīlauea melts and would require MI entrapment pressures of 10–25 kbar (depths exceeding 30–75 km). Furthermore, many bubble-dominated MI are located in close proximity to other MI that are either bubble-free or contain small bubbles (<5 vol%) and have similar major element glass compositions and total MI CO_2 concentrations generally <1000 ppm (Fig. 2). The elevated CO_2 densities in bubbles of bubble-dominated MI also indicate that these large bubbles formed by the co-entrapment of a separate CO_2-rich fluid phase rather than from MI decrepitation (which would have reduced CO_2 densities [Lowenstern, 2003]).

Steele-MacInnis et al. (2017) demonstrated that bubble-dominated MI with bubble volumes >~20% can generally be treated as isolated FI for calculating trapping pressures because the large mass of CO_2 in the

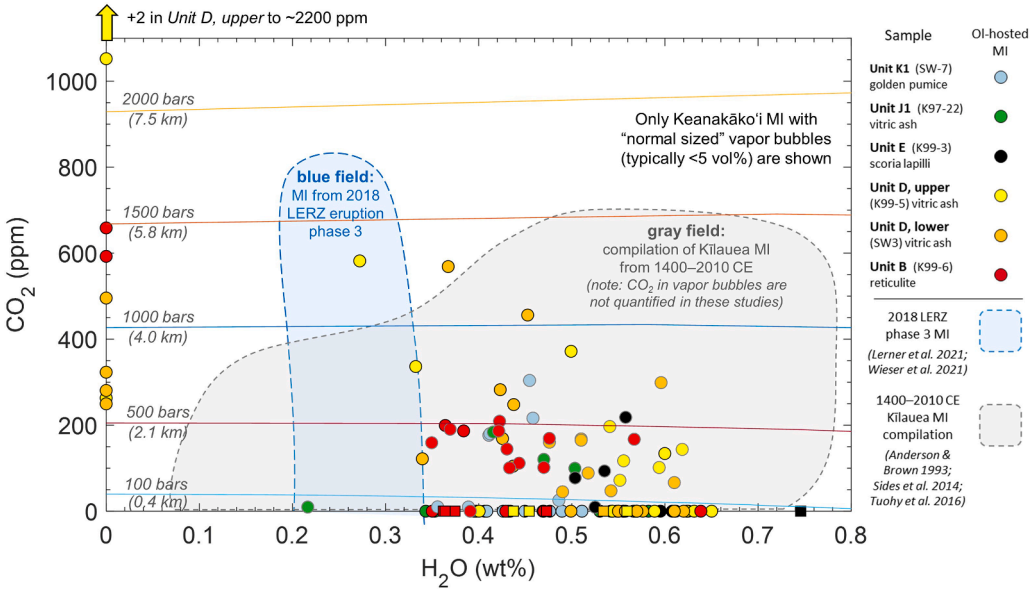

Fig. 2. H_2O-CO_2 measurements of Keanakāko'i melt inclusions (MI) analyzed in this study. Only bubble-free MI or MI with small vapor bubbles (<5 vol%) are shown. Samples plotting on the x- and y-axes lack CO_2 or H_2O measurements, respectively. Melt inclusion H_2O-CO_2 contents in Keanakāko'i MI are similar to MI in many other high-temperature Kīlauea magmas (gray field), and typically have higher H_2O than MI from phase 3 (high-temperature phase) of the 2018 lower East Rift Zone eruption (LERZ; blue field). General isobars shown are calculated for a 2018 lower East Rift Zone phase 3 matrix glass composition at 1150 °C using the solubility model of Iacono-Marziano et al. (2012). Data sources are listed within the figure.

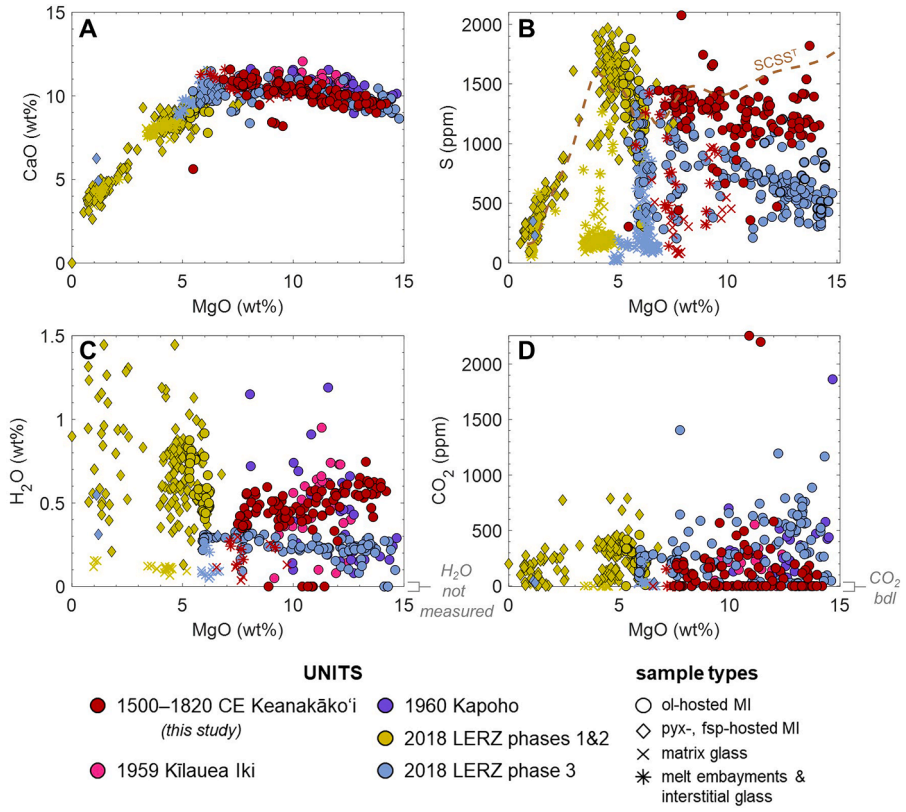

Fig. 3. CaO, sulfur, H_2O, and CO_2 vs MgO in Kīlauea melt inclusions (MI) and matrix glasses from Keanakāko'i Tephra units (this study; all units combined) compared to other Kīlauea samples: 2018 lower East Rift Zone (LERZ; Wieser et al., 2021, 2022; Lerner et al., 2021a), 1960 Kapoho (Tuohy et al., 2016), and 1959 Kīlauea Iki (Anderson and Brown, 1993; Tuohy et al., 2016). All MI data have been corrected for post-entrapment crystallization, if appropriate. The dashed brown curve in *(B)* is a parameterized down-temperature model of total sulfur concentration at sulfide saturation (SCSS^T) for Kīlauea melts taken from Lerner et al. (2021a).

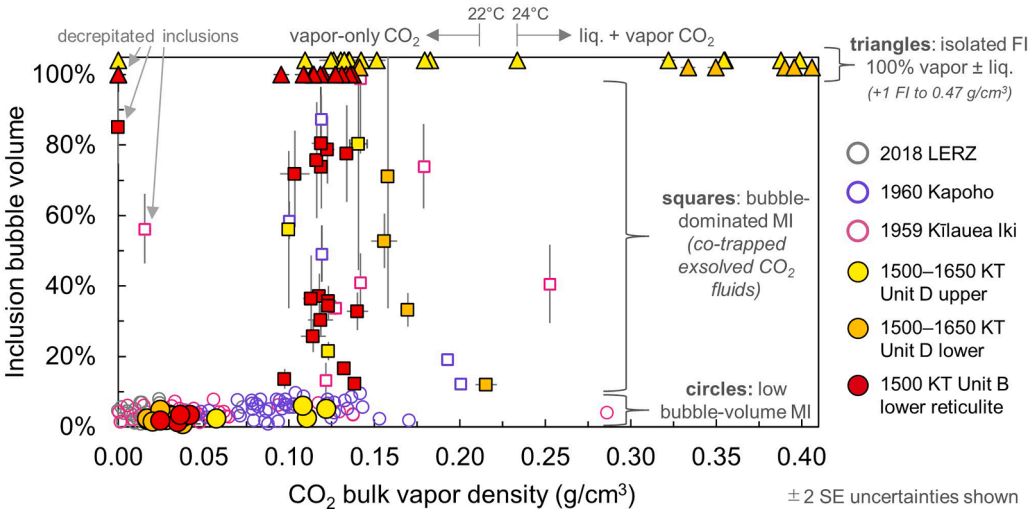

Fig. 4. CO_2 densities and vapor bubble volumes in melt inclusions (MI, circles) and isolated fluid inclusions (FI, triangles) from the Keanakāko'i Tephra (KT; this study), 1959 Kīlauea Iki and 1960 Kapoho (Moore et al., 2015), and 2018 lower East Rift Zone (LERZ) eruptions (Lerner et al., 2021a). Bubble-dominated MI (>10 vol% bubble; squares) have consistently high bubble CO_2 densities that resemble those of isolated FI, indicating they are co-entrapped CO_2-rich fluids. Large bubbles with low CO_2 densities have likely decrepitated. At room temperature (~22–24 °C), inclusions with CO_2 densities less than ~0.23 g/cm^3 contain only vapor-phase CO_2, whereas inclusions with CO_2 densities between ~0.23 and 0.74 g/cm^3 will contain both vapor- and liquid-phase CO_2. Error bars show ±2 standard error (SE); uncertainties of most CO_2 density measurements are smaller than symbol sizes.

bubble buffers changes in MI volume during cooling and quenching (further described in Supplementary Materials). Following this approach, we treat bubble-dominated MI as isolated FI and calculate their entrapment pressures using a CO_2 equation-of-state. When calculated this way, we find excellent agreement between barometry results from bubble-dominated MI and those of isolated FI and normal MI within individual crystals and between different crystals in the same unit (Figs. 5, 6), providing validation of this approach.

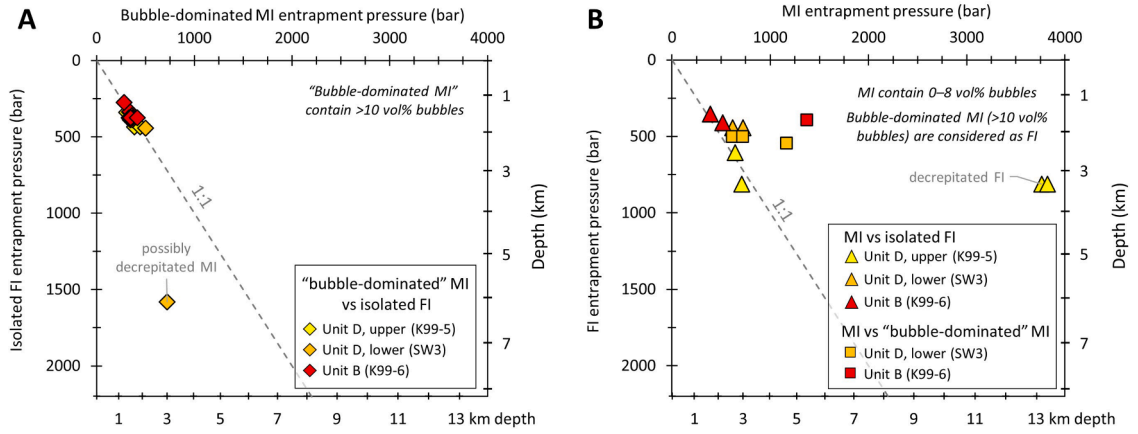

Fig. 5. *(A)* Entrapment pressures of bubble-dominated (i.e., >10 vol% bubble) melt inclusions (MI) and isolated fluid inclusions (FI) from Keanakāko'i units B, upper-D, and lower-D that co-occur within the same olivine crystal (see examples in Fig. 1). Pressures were calculated using CO_2 equation-of-state relations for both vapor bubbles in bubble-dominated MI and for isolated FI. *(B)* Entrapment pressures of normal MI (i.e., bubble-free, or with small bubbles) calculated using H_2O-CO_2 solubility models, compared to CO_2 equation-of-state barometry of bubbles in isolated FI (square symbols) and bubble-dominated MI (triangular symbols) that co-occur within the same olivine crystal. Entrapment pressures calculated from MI and FI in the same grain generally agree, with exceptions in FI that were visibly decrepitated (Fig. 1H, Figure S7).

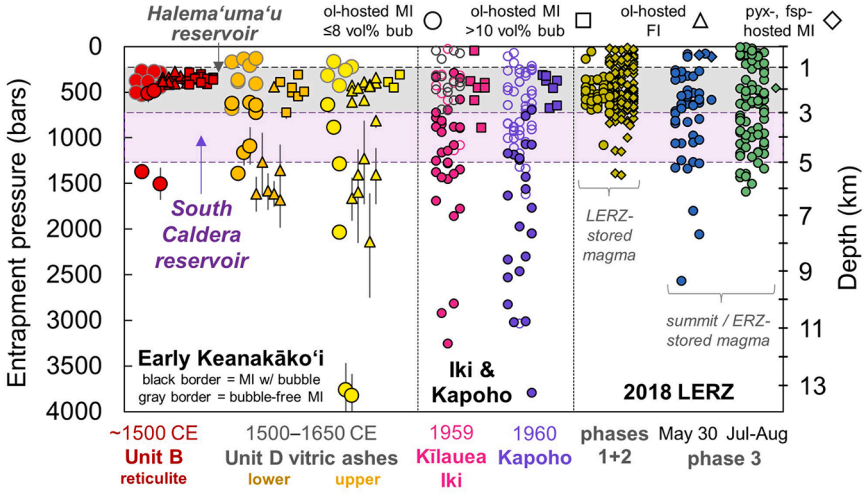

Fig. 6. Entrapment pressures for Kīlauea samples from 1500 to 2018 CE based on the total CO_2 content of melt inclusions (MI, circles), and CO_2 densities of isolated fluid inclusions (FI, triangles) and MI containing co-entrapped CO_2 fluid (MI with >10 vol% bubbles; squares). All inclusions are olivine-hosted except for 2018 lower East Rift Zone (LERZ) samples, which also contain pyroxene- and feldspar-hosted MI (diamonds). Bubble-free MI from Keanakāko'i and Kīlauea Iki samples have gray symbol outlines. Keanakāko'i data: this study; Kīlauea Iki and Kapoho data: Anderson and Brown (1993) - bubble-free MI (unfilled gray circles), Moore et al. (2015) - CO_2 bubbles in MI by Raman (filled pink and purple circles), and Tuohy et al. (2016) - rehomogenized MI (unfilled pink and purple circles); 2018 LERZ: Lerner et al. (2021a) and Wieser et al. (2021). Further details in Supplementary Materials. Note: one MI from Kīlauea Iki with an anomalously high entrapment pressure of 5300 bars (~19 km depth) measured by Moore et al. (2015) is off-scale.

3.2. Pressure and depth calculations

H_2O-CO_2 saturation pressures were calculated using the composition-dependent solubility model of Iacono-Marziano et al. (2012) and implemented through the VESIcal tool (Iacovino et al., 2021). Entrapment pressures of FI and bubble-dominated MI were calculated from CO_2 bubble densities using the CO_2 equation-of-state model of Sterner and Pitzer (1994). To relate pressure to depth beneath the surface, we apply an updated depth-rock density model for Kīlauea based on Denlinger and Flinders (2022) (details in Supplementary Materials).

In the Keanakāko'i Unit B reticulite, bubble-free and low-bubble volume ("normal") MI in $Fo_{82–84}$ olivine have H_2O-CO_2 saturation pressures of 270–1500 bars (corresponding to depths of 1.2–5.8 km), and CO_2 barometry from FI and bubble-dominated MI in $Fo_{81–84}$ olivine yields entrapment pressures of 280–420 bars (1.2–1.8 km) (Figs. 6, 7). In the lower-Unit D vitric ash, entrapment pressures of normal MI in $Fo_{82–89}$ olivine are 140–1390 bars (0.6–5.4 km) and entrapment pressures of FI and bubble-dominated MI in $Fo_{87–89}$ olivine are 440–1680 bars (1.9–6.4 km). In the upper-Unit D vitric ash, entrapment pressures of normal MI in $Fo_{86–89}$ olivine are 170–3800 bars (0.7–13.5 km) and entrapment pressures of FI and bubble-dominated MI in $Fo_{88–89}$ olivine are 310–2140 bars (1.3–7.9 km).

Where single crystals contain multiple types of inclusions (i.e., bubble-free MI, "normal" MI, bubble-dominated MI, isolated FI), the entrapment pressures of all types of (non-decrepitated) inclusions are very consistent (Fig. 5), indicating their co-formation. Within each unit, the overall ranges of MI and FI entrapment pressures are notably similar (Fig. 6). The close agreement between MI and FI barometric results, which are calculated using independent models (H_2O-CO_2 solubility in melts vs. CO_2 equation-of-state calculations), demonstrates that the chosen solubility models and input conditions (e.g., magma

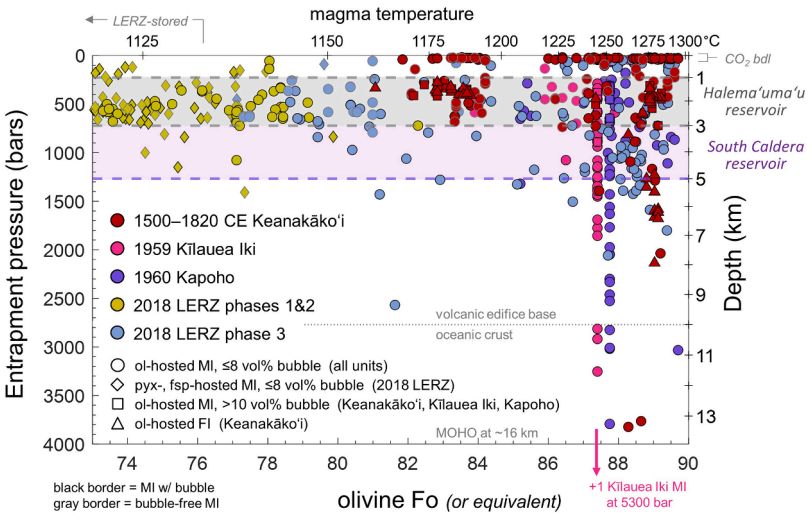

Fig. 7. Kīlauea melt inclusion (MI) and fluid inclusion (FI) entrapment pressures and mineral host compositions from 1500 to 2018 CE. Data sources as in Fig. 6, with combined unit symbology. Bubble-free MI have gray symbol outlines. Approximate magma temperatures for inclusions are shown at top (details in Supplementary Materials). Shallowly entrapped inclusions in high-temperature olivine are common in all investigated eruptions.

temperature) are appropriate for these magmas. Additionally, the agreement in entrapment pressures of MI and FI indicates that FI in these Keanakāko'i units did not experience significant post-entrapment modification (e.g., inclusion stretching, decrepitation, or significant H_2O leakage). Similarly, in samples from Kīlauea's 2018 lower East Rift Zone eruption, DeVitre and Wieser (accepted) find close agreement between MI and FI barometric results and use models of FI re-equilibration processes to demonstrate that post-entrapment modification of FI is relatively minor at Kīlauea over years-long timescales. This apparent lack of post-entrapment modification of FI at Kīlauea contrasts with observations at some volcanic systems with deeper magmatic storage areas, which have widespread evidence for FI modification and re-equilibration (e.g., Zanon and Frezzotti, 2013; Lo Forte et al., 2023; Dayton et al., 2023).

Collectively, these MI and FI results demonstrate that $Fo_{82–89}$ olivine from the early Keanakāko'i eruptions commonly crystallized at shallow depths of 1–3 km (Figs. 6, 7). Some high-Fo ($Fo_{86–89}$) olivine with bubble-bearing MI and two-phase (vapor + liquid CO_2) FI have deeper crystallization depths of 5–8 km.

4. Discussion

4.1. Storage depths of Kīlauea magma (1500–2018 CE)

The shallow 1–3 km range for crystallization of Keanakāko'i magmas is similar to common entrapment depths of MI and FI from modern eruptions (1959 Kīlauea Iki, 1960 Kapoho, 2018 lower East Rift Zone [Anderson and Brown, 1993; Moore et al., 2015; Tuohy et al., 2016; Lerner et al., 2021a; Wieser et al., 2021; DeVitre and Wieser, accepted]) and aligns with the depth of the geophysically identified Halema'uma'u magma reservoir (Poland et al., 2014; Anderson et al., 2019) (Figs. 6, 7). These data suggest that shallow magma crystallization and storage has been a relatively constant feature beneath Kīlauea's summit for at least 500 years, spanning both an explosive and effusive period.

Although these shallow depths match those of the modern Halema'uma'u reservoir, it does not necessarily indicate that a single large magma reservoir has been active over the last 500 years. For example, the large-scale caldera collapse preceding the Keanakāko'i period could have disrupted the upper magmatic plumbing system (Swanson and Houghton, 2019), causing subsequent shallow magma storage to occur in discrete, laterally separate bodies, which may have individually been intermittent features experiencing variable amounts of shallow fractional crystallization (Lynn et al., 2017; Garcia et al., 2018).

Deeper magma storage in the 3–5 km range has also been found for many MI from the 1959 Kīlauea Iki, 1960 Kapoho, and 2018 lower East Rift Zone eruptions, which aligns with the depth of the large geophysically identified South Caldera reservoir (Poland et al., 2014). However, for the early Keanakāko'i samples analyzed here, there is a paucity of MI and FI with entrapment depths in this 3–5 km range. Instead, many Keanakāko'i olivine crystals have crystallization depths of 5–8 km (Figs. 6, 7), which suggests that mid-crustal zones of eruptible magma during the early Keanakāko'i era were deeper than today's South Caldera reservoir depths. Some amount of deeper magma storage during the Keanakāko'i period had been previously proposed based on geochemical modeling (Helz et al., 2015; Lynn et al., 2017), and our barometry results provide direct evidence to support these interpretations.

Finally, numerous inclusions in olivine from the Keanakāko'i Unit D vitric ash samples and from the 1959 Kīlauea Iki and 1960 Kapoho eruptions (Moore et al., 2015; Tuohy et al., 2016) indicate crystallization depths of ≥5 km, suggesting that deeply sourced magmas contributed appreciably to these particular eruptions. The deepest entrapment depths that we measured in Keanakāko'i inclusions are from the upper-Unit D vitric ash, where one MI and one FI have entrapment depths of ~8 km and two MI in a single olivine crystal have entrapment depths of nearly 14 km. However, inclusions entrapped at depths >8 km are quite rare among our analyzed Keanakāko'i samples, with most MI and FI entrapment depths indicating storage dominantly at upper- to mid-crustal depths (1 to 8 km) rather than deeper storage at the base of the edifice (~10 km; Cayol et al., 2000) or the base of the crust (~16 km; Hill and Zucca, 1987). Some eruptions, such as the 2018 lower East Rift Zone eruption (phase 3; $Fo_{78–89}$) (Lerner et al., 2021a; Wieser et al., 2021; DeVitre and Wieser, accepted) and the Keanakāko'i Unit B reticulite ($Fo_{81–83}$) contain very few olivine with crystallization depths >5 km, suggesting that certain Kīlauea eruptions are almost entirely sourced from magma stored at shallow depths. However, we did not find or analyze high-Fo olivine in Keanakāko'i Unit B that have been previously identified (Sides et al., 2014; Lynn et al., 2017; Mourey et al., 2022), so further barometric investigation into the primitive components of this unit is warranted.

By linking olivine crystallization temperatures (see Supplementary Materials) with MI and FI entrapment pressures, we can assess the thermobarometric conditions of Kīlauea magma storage (Fig. 7). The vast majority of MI and FI in lower-temperature minerals in Keanakāko'i units ($Fo_{\leq 84}$ olivine) and in the 2018 lower East Rift Zone eruption (pyroxene, feldspar, and $Fo_{\leq 84}$ olivine; Lerner et al., 2021a; Wieser

et al., 2021, 2022; DeVitre and Wieser, accepted) were entrapped at shallow depths (≤3 km), indicating that evolved magmas are stored shallowly at Kīlauea. Melt and fluid inclusions entrapped at deeper depths (5 to >10 km) in all analyzed Keanakāko'i and modern Kīlauea samples are almost exclusively hosted in high-Fo olivine ($Fo_{86–89}$), confirming that deep magmas at Kīlauea are primitive (Moore et al., 2015; Tuohy et al., 2016; Wieser et al., 2021; Lerner et al., 2021a; this study).

However, we also find many inclusions in high-Fo olivine from Keanakāko'i and modern Kīlauea eruptions that have shallow entrapment depths of ≤3 km (Anderson and Brown, 1993; Moore et al., 2015; Tuohy et al., 2016; Wieser et al., 2021; Lerner et al., 2021a; DeVitre and Wieser, accepted; this study). This indicates that for at least 500 years, high-temperature magmas (1200–1300 °C) have regularly ascended to shallow depths beneath Kīlauea's summit, where they exist unmixed for sufficient time to crystallize high-temperature olivine. This notable observation alters the common assumption at Kīlauea (and other volcanoes) that the eruption of high-Fo olivine requires the rapid ascent of deeply stored magma with limited upper-crustal storage.

4.2. *Are the primitive magmas of the Keanakāko'i era unusual?*

Low entrapment pressures of MI and FI in high-Fo olivine are common to both explosive and effusive eras at Kīlauea, indicating that the injection and storage of high-temperature magmas at shallow depths occurs regularly. The presence of high-Fo olivine in more-evolved magmas from recent summit eruptions of Kīlauea (2008–2018, 2020–2021 CE; Lynn and Swanson, 2022; Mourey et al., 2023) demonstrates this ongoing process of primitive magma injection to shallow depths. More extensive evidence for the ascent of primitive magmas into shallow Kīlauea reservoirs is likely masked due to the rapid re-equilibration of high-Fo olivine in lower-temperature magmas (Mourey et al., 2023). The presence of high-temperature magmas at shallow depths during the Keanakāko'i era was therefore not particularly unusual for Kīlauea.

However, what is unusual about the Keanakāko'i eruptions is their eruption style, much lower magma flux, and preponderance of high-Fo olivine and high-temperature magma compositions compared to modern eruptions. We suggest that the latter was due to high-temperature magmas not undergoing extensive mixing and hybridization with

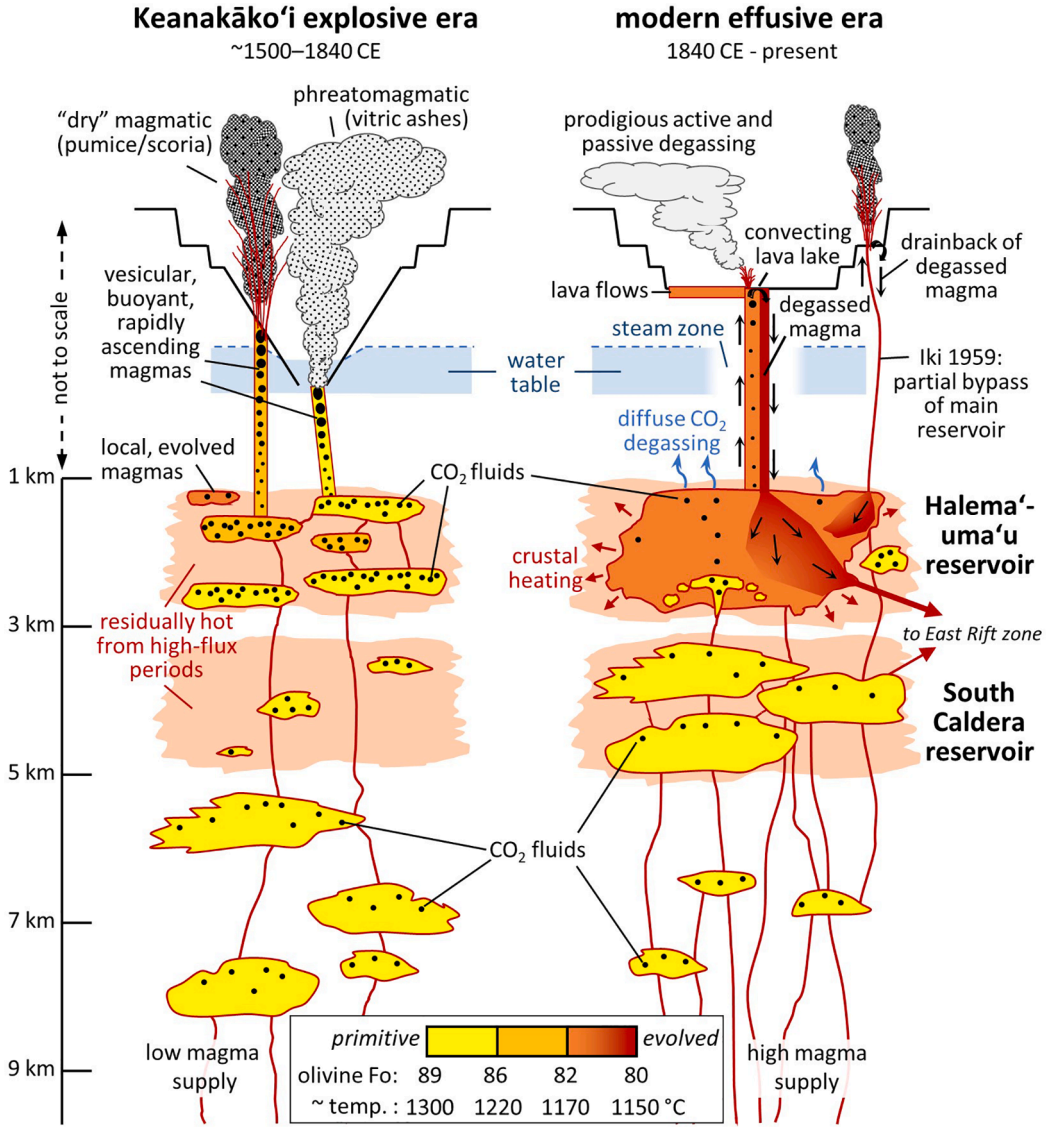

Fig. 8. Conceptual model of Kīlauea's magmatic system architecture during the Keanakāko'i era and the modern effusive era. Processes affecting exsolved volatiles and differences in explosive behavior are highlighted. Magma colors indicate primitive or evolved compositions (yellow = hotter, red = cooler) and the Fo composition of crystallizing olivine. See text for discussion.

evolved magmas, thus preserving their more-primitive signatures. Although clear signs of mixing are present in many Keanakāko'i samples (e.g., hybridized melts and bimodal olivine populations; Helz et al., 2015; Lynn et al., 2017; Garcia et al., 2018), mixing was much less extensive than in modern eruptions, where fewer high-Fo olivine are present and the current shallow magmatic system is dominated by lower-temperature magma (Thornber et al., 2015; Lerner et al., 2021a).

One mechanism to explain the less-extensive mixing of Keanakāko'i-era magmas is that the amount of hybridizing lower-temperature magma present beneath the summit was greatly reduced due to vast outpouring of summit-stored magma during the 'Ailā'au lava flows preceding the ~1500 CE caldera collapse (Swanson et al., 2012). Consequently, the more-evolved hybridizing magma was largely vacated from the summit area prior to the Keanakāko'i era, which enabled high-temperature magma injection into the upper crust to retain more of its primitive composition (Fig. 8). In addition, cooling rates of 1–5 °C/yr estimated for intrusions in Kīlauea's upper crust (Wright and Helz, 1996) and rapid diffusive re-equilibration timescales of olivine (Mourey et al., 2022) require that primitive Keanakāko'i magmas had relatively short residence times in shallow reservoirs (<~10 years) in order to crystallize and preserve the abundant high-Fo olivine that occur in Keanakāko'i eruptive products.

4.3. Magma storage depths at Kīlauea in a global context

Our results show that the depths and thermal structure of the shallow Kīlauea magmatic system were not radically different during explosive (low-flux) and effusive (high-flux) eras: both eras involved similar shallow storage at 1–3 km depth and mid-crustal storage zones only slightly deepened during the low-flux era (5–8 km) compared to the modern high-flux era (3–5 km). The common shallow storage zone (1–3 km) that existed during both low- and high-flux eras at Kīlauea contrasts with more substantial differences observed at mid-ocean ridge systems and in Iceland, where shallow reservoirs dominate in higher-flux systems and become deeper in lower-flux systems (Soule, 2015; Baxter et al., 2023). However, the shallowing mid-crustal magma storage between the Keanakāko'i era compared to the modern era is consistent with a slight deepening of magma storage in response to the decrease in flux.

The dominantly shallow magma storage at Kīlauea is similar to magma storage depths as shallow as ~2 km at Sierra Negra (Galapagos; Bell et al., 2021) and 3–5 km at Piton de la Fournaise (Reunion Island; Bureau et al., 1998; Peltier et al., 2015), which are two other intraplate volcanoes with high magma supply. Such shallow magma storage zones are typically absent in intraplate volcanoes with lower magma fluxes (e.g., magma storage depths of 7–25 km at Fogo [Cape Verde; Hildner et al., 2012] and Haleakala [Maui; Moore et al., 2021], and up to 30 km at Ross Island [Antarctica; Rasmussen et al., 2017] and Cumbre Vieja [Canary Islands; Dayton et al., 2023]). High magma supply rates at Kīlauea and other frequently active intraplate oceanic systems are likely critical in maintaining a hot upper crust that enables shallower crustal storage.

Our barometry results indicate that during low-flux explosive periods at Kīlauea, high-temperature magmas still accumulate at depths ≤3 km. This raises an interesting question as to how magma storage depths vary in response to a change from high to low magma flux. The global patterns summarized above suggest that magma storage depths would deepen considerably in response to decreased magma flux. However, Kīlauea does not strongly follow this trend during its low magma flux (explosive) periods. Similarly, there are several examples of low-flux basaltic volcanoes in southern Iceland that appear to have very shallow magma storage. This has been attributed to lithospheric stretching and thinning that precedes development of an active rift system, resulting in a warmer thermal structure in the crust (Baxter et al., 2023).

We suggest that during periods of high magma supply at Kīlauea (i.e., effusive eras, such as the 1000–1500 CE "Observatory Shield" era prior to the Keanakāko'i sequence, and the post-1840 CE modern era; Swanson et al., 2014) the upper crust was extensively heated due to the large volumes of magma present at shallow levels, which provided sufficient thermal mass to prevent rapid cooling and fractionation of incoming high-temperature magma during subsequent periods of low magma supply (i.e., explosive eras) (Fig. 8). Given the geologically short (centuries-long) timescales of explosive and effusive eras at Kīlauea and the low thermal diffusivity of rocks, the residual heat from the thermally primed crust likely helped shallow storage of basaltic magma to persist. Small injections of primitive magma during low-flux eras could hereby remain at high temperatures for much longer than if injected into a cold upper crust.

4.4. CO_2-rich magmatic fluids and controls on summit eruptive energetics

The energetic Keanakāko'i eruptive period began following a ≥600 m deep caldera collapse (Swanson et al., 2012). Deep summit calderas are likely related to explosive eruptive styles at Kīlauea because they can host groundwater-fed lakes (Mastin, 1997; Mastin et al., 2004), and many Keanakāko'i units have hydromagmatic textural features indicating interaction with external water (McPhie et al., 1990; Mastin et al., 2004; Swanson and Houghton, 2019; Schmith and Swanson, 2023). The formation of a groundwater-fed lake within the deepened Halema'uma'u Crater following the 2018 caldera collapse demonstrated this process of lake formation when Kīlauea's caldera floor drops below the groundwater table (Nadeau et al., 2020; Ingebritsen et al., 2021). However, other Keanakāko'i units were energetic "dry" eruptions lacking an influence from external water (Units B reticulite and Units K1 and K2 basaltic pumice from ≥500 m-high lava fountains, and Unit E scoria lapilli; Swanson and Houghton, 2019), where the high eruption energies were driven by characteristics of the magma itself. We hypothesize that accumulated CO_2-rich exsolved fluids were an important driver that contributed to both Keanakāko'i magmatic and hydromagmatic eruptions.

Considering the high initial CO_2 in Kīlauea magmas (≥0.7 wt%; Gerlach et al., 2002; Anderson and Poland, 2017), CO_2 will begin exsolving within the mantle at depths of ~30 km. In contrast, large-scale H_2O and S exsolution from Kīlauea magmas only occurs at near-surface depths (≤200 m; Gerlach, 1986; Lerner et al., 2021a), meaning that CO_2 is the main exsolving volatile during the majority of magma ascent beneath Kīlauea. CO_2-rich FI with entrapment depths up to 8 km in Keanakāko'i olivine are direct evidence of deeply exsolving supercritical CO_2 fluids. The importance of deeply exsolved CO_2-rich fluids ascending through a trans-crustal magma system has been recognized at many volcanoes worldwide both petrologically (e.g., Roedder, 1965) and in surface gas emissions (e.g., Werner et al., 2019), and increases in CO_2/S and CO_2/H_2O ratios in gas emissions have been used to identify deep magma recharge (e.g., Aiuppa et al., 2021).

Although our observations of abundant CO_2-rich FI in Keanakāko'i olivine demonstrate the presence of CO_2-rich fluids over a wide range of depths beneath Kīlauea, the presence of such FI have only rarely been reported in previous Kīlauea literature. To assess whether FI in Keanakāko'i units are anomalous compared to other Kīlauea eruptive periods, we examined tens to hundreds of phenocrysts from modern Kīlauea eruptions and found that magmatic FI are present in all investigated units (Figure S5). These FI from modern eruptions are almost all vapor-phase, indicating entrapment at depths <~3 km (see discussion in Supplementary Materials on the use of optical petrography for rapid barometric estimates of CO_2-dominated FI), consistent with the common shallow storage depths of these units based on MI barometry, and with recent FI barometry from the 2018 lower East Rift Zone eruption (DeVitre and Wieser, accepted).

Importantly, the abundance of FI varies substantially across different Kīlauea eruptions: very small FI (≤30 μm diameters) are present in <5% of phenocrysts in 2018 lower East Rift Zone samples, ≤15% of olivine

from 1960 Kapoho, and ~50% of Kīlauea Iki olivine. In comparison, FI are present in >25% of olivine in Keanakāko'i units, including ~60% of olivine in highly vesicular Units B and K1. Keanakāko'i FI are also notably larger (up to 150 μm diameters) than FI in modern eruptions. Because the dominantly shallow magma storage depths, olivine textures, and MI textures of Keanakāko'i and modern Kīlauea samples are generally similar, the abundance and size of FI in Keanakāko'i units suggest that the magmas likely contained a greater volume fraction of exsolved CO_2-rich fluid during olivine growth (see discussion in Supplementary Materials).

Due to the high initial CO_2 concentrations of Kīlauea magmas and the low solubility of CO_2 at shallow pressures, isothermal magma ascent from the mantle to upper crustal magma reservoirs would result in ~92 and ~97% of initial CO_2 being exsolved by the time magma reached respective depths of 5 and 2 km (details in Supplementary Materials). Considering the pressure-dependent density of CO_2 fluids in high-temperature magmas (e.g., 0.15 and 0.33 g/cm^3 at 2 and 5 km, respectively, at 1250 °C; Sterner and Pitzer, 1994) compared to the density of basaltic magma (~2.70 g/cm^3), fully closed-system degassing behavior during ascent would result in exsolved CO_2 fluids making up ~5 vol% of the magma at 5 km depths and ~11 vol% at 2 km depths. Changes through time in the degree of open- vs closed-system outgassing behavior could strongly affect the exsolved CO_2 fluid fractions remaining in Kīlauea's upper crustal reservoirs, with implications for magma compressibility, buoyancy, and potential eruption energy.

Since the mid-1800s, efficient gas release and convective recycling from persistent lava lake activity (1840–1894, 1906–1924, 2008–2018 CE) and lava drainback from frequent summit eruptions (e.g., Wright and Klein, 2014) likely prevented the accumulation of CO_2-rich fluids in magma beneath Kīlauea's summit (Lerner et al., 2021a). Even during periods of eruptive quiescence, large fluxes of 8–20 kt/day of CO_2 have been emitted at Kīlauea's summit (Gerlach et al., 2002; Sutton and Elias, 2014), demonstrating that exsolving CO_2 has been readily escaping to the surface at Kīlauea's summit during the modern effusive era. This open-system outgassing (i.e., passive degassing) of CO_2 in the modern Kīlauea era reduces the likelihood of volatile accumulation and FI entrapment in shallow magma reservoirs.

However, following large-scale caldera collapses, such as in ~1500 CE, outgassing pathways to the surface likely change and may become blocked. Additionally, inferred magma fluxes during explosive eras following caldera collapses are significantly decreased (Swanson et al., 2014) and the deepened calderas may become filled with groundwater-fed lakes; both of these processes reduce the likelihood of persistent lava-lake activity and thereby minimize convective outgassing and the recycling of volatile-depleted magma back into the deeper system. Furthermore, the low magma flux during the Keanakāko'i era seems related to decreased mantle melting fractions (Mourey et al., 2022), which may have caused Keanakāko'i magmas to be inherently enriched in CO_2 and other incompatible elements (Sides et al., 2014).

Collectively, these processes occurring during the Keanakāko'i era could have led to abundant CO_2-rich fluids exsolving from ascending magmas and accumulating in inefficiently outgassing shallow magma storage zones (particularly at 1–3 km depths, based on our FI barometry) (Fig. 8). The presence of accumulated CO_2-rich fluids would increase magma buoyancy and enhance magma ascent rates, and has been proposed to play an important role in driving basaltic eruptions (e.g., Allison et al., 2021; Aiuppa et al., 2021; DeVitre et al., 2023b). Volatile diffusion profiles in melt embayments in Keanakāko'i olivine indicate that the final ascent of magma from storage at 2–4 km to the surface occurred within tens of minutes, and these rapid ascent rates require the presence of exsolved fluids at depth (Ferguson et al., 2016). These take-off depths and the presence of an "excess" fluid phase are consistent with our MI and FI evidence for shallow Keanakāko'i magma reservoirs that contained substantial fractions of accumulated exsolved CO_2-rich fluids. Rapidly ascending, vesicular, CO_2-buoyed magma would power more energetic eruptive behavior, including promoting vigorous magma interaction and heat exchange with external water that could have contributed to the repeated episodes of powerful hydromagmatic explosions in deepened calderas during the Keanakāko'i period (Mastin et al., 2004).

This hypothesis of CO_2-charged magmas contributing to the explosivity of Keanakāko'i eruptions may also be relevant for older explosive episodes at Kīlauea, such as the Uēkahuna and Pahala Ash sequences (e.g., Fiske et al., 2019). Examining FI abundance and barometry in these older explosive units would help identify whether shallow magma storage and increased exsolved CO_2-rich fluids are common features of explosive eras at Kīlauea. Increased focus on CO_2-rich FI could also be applied to other Hawaiian volcanoes and volcanoes globally to better understand magmatic storage conditions and the role of exsolved CO_2 in influencing eruption styles.

5. Conclusions

1) In presenting new melt inclusion (MI) and fluid inclusion (FI) data from the Keanakāko'i eruptive sequence (1500–1840 CE), we expand the dataset of barometric measurements at Kīlauea to span the last 500 years. We find that shallow magma storage at depths of 1–3 km has persisted throughout both the explosive Keanakāko'i era and the modern effusive era. However, mid-crustal magma storage has seemingly shallowed from depths of 5–8 km during the explosive Keanakāko'i era to depths of 3–5 km during the modern period. In the modern era, these petrologically determined upper and mid-crustal magma storage depths are in good agreement with geophysical observations of the shallow Halema'uma'u and deeper South Caldera reservoirs.

2) Throughout the last 500 years of Kīlauea eruptions, we commonly find high-Fo ($Fo_{86–89}$) olivine containing MI and FI that have shallow entrapment depths of 1–3 km. This indicates that high-temperature magmas (>1200 to ~1300 °C) regularly ascend to, and crystallize at, shallow depths during both explosive (low-magma flux) and effusive (high-magma flux) eruptive periods. These results challenge a standard paradigm in petrology that high-temperature, primitive melts only crystallize in the deep crust or uppermost mantle and do not commonly ascend into (or last very long unmodified in) the colder upper crust.

3) Fluid inclusions are present in minerals from every Kīlauea eruption that we investigated, but FI are both larger and far more abundant in olivine from the Keanakāko'i era compared to effusive eruptions of the modern era (e.g., 1960 Kapoho, 2018 lower East Rift Zone). The increased abundance of CO_2-dominated FI in Keanakāko'i olivine may reflect increased amounts of exsolved CO_2 fluids in these magmas, which could result from a lack of open-system conduits to the surface during this era of low magma flux and smaller, more ephemeral magma bodies. Greater amounts of CO_2-rich fluid would have increased magma buoyancy and ascent rates, leading to enhanced interaction with shallow water bodies and greater explosivity of Keanakāko'i eruptions.

4) We demonstrate the utility of a combined MI and FI study and find excellent agreement between barometry calculations using H_2O-CO_2 volatile solubilities in MI and CO_2 equation-of-state calculations in isolated FI and in co-trapped exsolved fluid bubbles within MI (i.e., bubble-dominated MI with >10 vol% bubble). Data from MI and FI in Keanakāko'i samples provide complementary data to better constrain melt temperature, melt and fluid compositions, exsolved fluid abundance, and to aid in the interpretation of large vapor bubbles in MI (e.g., formed endogenously or through co-entrapment of an exsolved fluid), assess post-entrapment modification of FI (e.g., stretching, decrepitation, H_2O leakage), and provide independent barometric methods to constrain magma storage depths. Coupled MI and FI studies have only rarely been conducted at active volcanoes (e.g., Bureau et al., 1998; Mironov and Portnyagin, 2011; Métrich et al., 2014; Simonov et al., 2021; Correale et al., 2024; DeVitre and Wieser, accepted) but can be undertaken at volcanic systems worldwide to provide valuable insights into plumbing system barometry and volatile behavior.

CRediT authorship contribution statement

Allan H. Lerner: Conceptualization, Data curation, Investigation, Methodology, Writing – original draft. **D. Matthew Sublett:** Investigation, Methodology, Data curation. **Paul J. Wallace:** Conceptualization, Funding acquisition, Resources, Writing – review & editing. **Christina Cauley:** Investigation, Writing – review & editing. **Robert J. Bodnar:** Investigation, Writing – review & editing.

Declaration of competing interest

The authors declare that they have no known competing financial interests or personal relationships that could have appeared to influence the work reported in this paper.

Acknowledgements

We thank Don Swanson, the late Fred Anderson, and staff of the Hawaiian Volcano Observatory for introducing us to the Keanakāko'i deposits and for invaluable fieldwork assistance and discussions. We are grateful to Nicole Métrich, Andrey Gurenko, and Jake Lowenstern for valuable comments that improved this manuscript, and to Chiara Maria Petrone for editorial handling. We also thank Kendra Lynn and two anonymous reviewers for constructive comments that improved an earlier version of this paper, and Dawn Hart for assistance with sample preparation and analysis. Funding was provided by National Science Foundation grant EAR-2020049. Any use of trade, firm, or product names is for descriptive purposes only and does not imply endorsement by the U.S. Government.

Supplementary materials

Supplementary material associated with this article can be found, in the online version, at doi:10.1016/j.epsl.2024.118579.

References

Aiuppa, A., et al., 2021. Volcanic CO_2 tracks the incubation period of basaltic paroxysms. Sci. Adv. 7, eabh0191. https://doi.org/10.1126/sciadv.abh0191.

Allison, C.M., Roggensack, K., Clarke, A.B., 2021. Highly explosive basaltic eruptions driven by CO_2 exsolution. Nat. Commun. 12, 217. https://doi.org/10.1038/s41467-020-20354-2.

Anderson, A.T., Brown, G.G., 1993. CO_2 contents and formation pressures of some Kilauean melt inclusions. Am. Mineral. 78, 794–803.

Anderson, K.R., Poland, M.P., 2017. Abundant carbon in the mantle beneath Hawai'i. Nat. Geosci. 10, 704–708 v. doi:10.1038/ngeo3007.

Anderson, K.R., Johanson, I.A., Patrick, M.R., Gu, M., Segall, P., Poland, M.P., Montgomery-Brown, E.K., Miklius, A., 2019. Magma reservoir failure and the onset of caldera collapse at Kīlauea Volcano. 2018: Science 366. https://doi.org/10.1126/science.aaz1822.

Aster, E.M., Wallace, P.J., Moore, L.R., Watkins, J., Gazel, E., Bodnar, R.J., 2016. Reconstructing CO_2 concentrations in basaltic melt inclusions using Raman analysis of vapor bubbles. J. Volcanol. Geotherm. Res. 323, 148–162. https://doi.org/10.1016/j.jvolgeores.2016.04.028, v..

Baxter, R.J.M., Maclennan, J., Neave, D.A., Thordarson, T., 2023. Depth of magma storage under Iceland controlled by magma fluxes: geochemistry. Geophysics, Geosystems 24, e2022GC010811. https://doi.org/10.1029/2022GC010811.

Bell, A.F., et al., 2021. Caldera resurgence during the 2018 eruption of Sierra Negra volcano, Galápagos Islands. Nature Communications, v 12, 1397. https://doi.org/10.1038/s41467-021-21596-4.

Bureau, H., Métrich, N., Pineau, F., Semet, M.P., 1998. Magma–conduit interaction at Piton de la Fournaise volcano (Réunion Island): a melt and fluid inclusion study. J. Volcanol. Geotherm. Res. 84, 39–60. https://doi.org/10.1016/S0377-0273(98)00029-8.

Cayol, V., Dieterich, J.H., Okamura, A.T., Miklius, A., 2000. High magma storage rates before the 1983 Eruption of Kilauea. Hawaii: Science 288, 2343–2346. https://doi.org/10.1126/science.288.5475.2343.

Correale, A., Corsaro, R.A., Miraglia, L., Paonita, A., Rotolo, S.G., 2024. The December 2018 eruption at Etna volcano: a geochemical study on melt and fluid inclusions: Front. Earth Sci. 11. https://doi.org/10.3389/feart.2023.1122132.

Danyushevsky, L.V., Plechov, P., 2011. Petrolog3: Integrated software for modeling crystallization processes. Geochemistry, Geophysics, Geosystems 12, Q07021. https://doi.org/10.1029/2011GC003516.

Dayton, K., et al., 2023. Deep magma storage during the 2021 La Palma eruption. Sci. Adv. 9, eade7641. https://doi.org/10.1126/sciadv.ade7641.

Decker, R.W., Christiansen, R.L., 1984. Explosive eruptions of Kilauea Volcano, Hawaii, in explosive volcanism: inception, evolution, and hazards. Studies in Geophysics Series. National Academy Press, pp. 122–132.

Denlinger, R.P., Flinders, A., 2022. Density structure of the island of Hawai'i and the implications for gravity-driven motion of the south flank of Kīlauea Volcano. Geophys. J. Int. 228, 1793–1807. https://doi.org/10.1093/gji/ggab398.

DeVitre, C.L., Wieser, P.E., accepted. Reliability of Raman analyses of CO2-rich fluid inclusions as a geobarometer at K..lauea. Geochemical Perspectives Letters. doi:10.7185/geochemlet.2404.

DeVitre, C.L., Dayton, K., Gazel, E., Pamukçu, A., Gaetani, G., Wieser, P.E., 2023a. Laser heating effect on Raman analysis of CO_2 co-existing as liquid and vapor in olivine-hosted melt inclusion bubbles. Volcanica 6, 201–219. https://doi.org/10.30909/vol.06.02.201219.

DeVitre, C.L., Gazel, E., Ramalho, R.S., Venugopal, S., Steele-MacInnis, M., Hua, J., Allison, C.M., Moore, L.R., Carracedo, J.C., Monteleone, B., 2023b. Oceanic intraplate explosive eruptions fed directly from the mantle. Proc. Natl. Acad. Sci. 120, e2302093120 https://doi.org/10.1073/pnas.2302093120.

Dixon, J.E., Stolper, E.M., Holloway, J.R., 1995. An experimental study of water and carbon dioxide solubilities in mid-ocean ridge basaltic liquids. Part I: calibration and solubility models. J. Petrol. 36, 1607–1631. https://doi.org/10.1093/oxfordjournals.petrology.a037267.

Easton, R.M., 1987. Stratigraphy of Kilauea Volcano. In: U.S. Geological Survey Professional Paper 1350, USGS Professional Paper, 1350, pp. 234–260. https://pubs.usgs.gov/pp/1987/1350/pdf/chapters/pp1350_ch11.pdf.

Sides, I.R., Edmonds, M., Maclennan, J., Swanson, D.A., Houghton, B.F., 2014. Eruption style at Kīlauea Volcano in Hawai'i linked to primary melt composition. Nat. Geosci. (7), 464–469 v. doi:10.1038/ngeo2140.

Ferguson, D.J., Gonnermann, H.M., Ruprecht, P., Plank, T., Hauri, E.H., Houghton, B.F., Swanson, D.A., 2016. Magma decompression rates during explosive eruptions of Kīlauea volcano, Hawaii, recorded by melt embayments. Bull. Volcanol. 78, 71. https://doi.org/10.1007/s00445-016-1064-x.

Fiske, R.S., Rose, T.R., Swanson, D.A., Champion, D.E., McGeehin, J.P., 2009. Kulanaokuaiki Tephra (ca. A.D. 400–1000): Newly recognized Evidence For Highly Explosive Eruptions At Kīlauea Volcano, 121. GSA Bulletin, Hawai'i, pp. 712–728. https://doi.org/10.1130/B26327.1.

Fiske, R.S., Rose, T.R., Swanson, D.A., Andrews, B.J., Nichols, A.R.L., 2019. The Kulanaokuaiki-3 tephra, 900 CE: Products of a Remarkably Energetic Pyroclastic Eruption At Kīlauea Volcano, 131. GSA Bulletin, Hawai'i, USA, pp. 1537–1554. https://doi.org/10.1130/B35063.1.

Frezzotti, M.-L., 2001. Silicate-melt inclusions in magmatic rocks: applications to petrology: lithos 55, 273–299. https://doi.org/10.1016/S0024-4937(00)00048-7.

Garcia, M.O., Mucek, A.E., Lynn, K.J., Swanson, D.A., and Norman, M.D., 2018, Geochemical evolution of Keanakāko'i Tephra, Kīlauea Volcano, Hawai'i, in Poland, M.P., Garcia, M.O., Camp, V., and Grunder, A. eds., Field Volcanology: A Tribute to the Distinguished Career of Don Swanson, Geological Society of America Special Paper, v. 536, doi:10.1130/2018.2538(09).

Gerlach, T.M., McGee, K.A., Elias, T., Sutton, A.J., Doukas, M.P., 2002. Carbon dioxide emission rate of Kīlauea Volcano: implications for primary magma and the summit reservoir. J. Geophys. Res. 107, ECV-3. https://doi.org/10.1029/2001JB000407.

Gerlach, T.M., 1986. Exsolution of H_2O, CO_2, and S during eruptive episodes at Kilauea Volcano, Hawaii. J. Geophys. Res. 91, 12177–12185. https://doi.org/10.1029/JB091iB12p12177.

Hansteen, T.H., Klügel, A., 2008. Fluid inclusion thermobarometry as a tracer for magmatic processes. Rev. Mineral. Geochem. 69, 143–177. https://doi.org/10.2138/rmg.2008.69.5.

Hanyu, T., Yamamoto, J., Kimoto, K., Shimizu, K., Ushikubo, T., 2020. Determination of total CO_2 in melt inclusions with shrinkage bubbles. Chem. Geol. 557, 119855 https://doi.org/10.1016/j.chemgeo.2020.119855.

Hartley, M.E., Maclennan, J., Edmonds, M., Thordarson, T., 2014. Reconstructing the deep CO_2 degassing behaviour of large basaltic fissure eruptions. Earth Planet. Sci. Lett. 393, 120–131. https://doi.org/10.1016/j.epsl.2014.02.031.

Helz, R.T., Thornber, C.R., 1987. Geothermometry of Kilauea Iki lava lake, Hawaii. Bull. Volcanol. 49, 651–668. https://doi.org/10.1007/BF01080357.

Helz, R.T., Clague, D.A., Mastin, L.G., Rose, T.R., 2015. Evidence for large compositional ranges in coeval melts erupted from Kīlauea's summit reservoir, in Hawaiian Volcanoes. AGU 125–145. https://doi.org/10.1002/9781118872079.ch7.

Hildner, E., Klügel, A., Hansteen, T.H., 2012. Barometry of lavas from the 1951 eruption of Fogo, Cape Verde Islands: implications for historic and prehistoric magma plumbing systems. J. Volcanol. Geotherm. Res. 217–218, 73–90. https://doi.org/10.1016/j.jvolgeores.2011.12.014.

Hill, D.D., and Zucca, J.J., 1987, Geophysical Constraints On the Structure of Kilauea and Mauna Loa Volcanoes and Some Implications For Seismomagmatic Processes, in Decker, R.W., Wright, T.L., and Stauffer, P.H. eds., Volcanism in Hawaii, U.S. Geological Survey Professional Paper, v. 1350, p. 903–917.

Iacono-Marziano, G., Morizet, Y., Le Trong, E., Gaillard, F., 2012. New experimental data and semi-empirical parameterization of H_2O–CO_2 solubility in mafic melts. Geochim. Cosmochim. Acta 97, 1–23. https://doi.org/10.1016/j.gca.2012.08.03.

Iacovino, K., Matthews, S., Wieser, P.E., Moore, G.M., Bégué, F., 2021. VESIcal Part I: an Open-Source Thermodynamic Model Engine for Mixed Volatile (H_2O-CO_2) Solubility in Silicate Melts. Earth Space Sci. 8, e2020EA001584 https://doi.org/10.1029/2020EA001584.

Ingebritsen, S.E., Flinders, A.F., Kauahikaua, J.P., Hsieh, P.A., 2021. Modeling groundwater inflow to the New Crater Lake at Kīlauea Volcano. Hawai'i: Groundwater 59, 7–15. https://doi.org/10.1111/gwat.13023.

Lerner, A.H., et al., 2021a. The petrologic and degassing behavior of sulfur and other magmatic volatiles from the 2018 eruption of Kīlauea, Hawai'i: melt concentrations,

magma storage depths, and magma recycling. Bull. Volcanol. 83, 43. https://doi.org/10.1007/s00445-021-01459-y.
Lerner, A.H., Muth, M.J., Wallace, P.J., Lanzirotti, A., Newville, M., Gaetani, G.A., Chowdhury, P., Dasgupta, R., 2021b. Improving the reliability of Fe- and S-XANES measurements in silicate glasses: correcting beam damage and identifying Fe-oxide nanolites in hydrous and anhydrous melt inclusions. Chem. Geol. 586, 120610 https://doi.org/10.1016/j.chemgeo.2021.120610.
Lo Forte, F.M., Aiuppa, A., Rotolo, S.G., Zanon, V., 2023. Temporal evolution of the Fogo Volcano magma storage system (Cape Verde Archipelago): a fluid inclusions perspective. J. Volcanol. Geotherm. Res. 433, 107730 https://doi.org/10.1016/j.jvolgeores.2022.107730.
Lowenstern, J.B., 2003. Melt inclusions come of age: volatiles, volcanoes, and sorby's legacy. In: De Vivo, B., Bodnar, R.J. (Eds.), Developments in Volcanology, Elsevier, Melt Inclusions in Volcanic Systems 5, 1–21. https://doi.org/10.1016/S1871-644X(03)80021-9.
Lynn, K.J., Swanson, D.A., 2022. Olivine and glass chemistry record cycles of plumbing system recovery after summit collapse events at Kīlauea Volcano, Hawai'i. J. Volcanol. Geotherm. Res. 426, 107540 https://doi.org/10.1016/j.jvolgeores.2022.107540.
Lynn, K.J., Garcia, M.O., Shea, T., Costa, F., Swanson, D.A., 2017. Timescales of mixing and storage for Keanakāko'i Tephra magmas (1500–1820 C.E.), Kīlauea Volcano. Hawai'i: Contributions to Mineralogy and Petrology 172, 76. https://doi.org/10.1007/s00410-017-1395-4.
Métrich, N., Zanon, V., Créon, L., Hildenbrand, A., Moreira, M., Marques, F.O., 2014. Is the 'Azores Hotspot' a Wetspot? Insights from the geochemistry of fluid and melt inclusions in olivine of pico basalts. J. Petrol. 55, 377–393. https://doi.org/10.1093/petrology/egt071.
Mastin, L.G., Christiansen, R.L., Thornber, C., Lowenstern, J., Beeson, M., 2004. What makes hydromagmatic eruptions violent? Some insights from the Keanakāko'i Ash, Kīlauea Volcano, Hawai'i. J. Volcanol. Geotherm. Res. 137, 15–31. https://doi.org/10.1016/j.jvolgeores.2004.05.015.
Mastin, L.G., 1997. Evidence for water influx from a caldera lake during the explosive hydromagmatic eruption of 1790, Kilauea volcano, Hawaii. J. Geophys. Res. 102, 20093–20109. https://doi.org/10.1029/97JB01426.
McPhie, J., Walker, G.P., Christiansen, R.L., 1990. Phreatomagmatic and phreatic fall and surge deposits from explosions at Kilauea volcano, Hawaii, 1790 AD. Keanakakoi Ash Member. Bulletin of Volcanology 52, 334–354. https://doi.org/10.1007/BF00302047.
Mironov, N.L., Portnyagin, M.V., 2011. H_2O and CO_2 in parental magmas of Kliuchevskoi volcano inferred from study of melt and fluid inclusions in olivine. Russ. Geol. Geophys. 52, 1353–1367. https://doi.org/10.1016/j.rgg.2011.10.007.
Moore, L.R., Gazel, E., Tuohy, R., Lloyd, A.S., Esposito, R., Steele-MacInnis, M., Hauri, E. H., Wallace, P.J., Plank, T., Bodnar, R.J., 2015. Bubbles matter: an assessment of the contribution of vapor bubbles to melt inclusion volatile budgets. Am. Mineral 100 v, 806–823, doi:10.2138/am-2015-5036.
Moore, L.R., Gazel, E., Bodnar, R.J., 2021. The volatile budget of Hawaiian magmatism: constraints from melt inclusions from Haleakala volcano, Hawaii. J. Volcanol. Geotherm. Res. 410, 107144 https://doi.org/10.1016/j.jvolgeores.2020.107144.
Mourey, A.J., Shea, T., Lynn, K.J., Lerner, A.H., Lambart, S., Costa, F., Oalmann, J., Lee, R.L., and Gansecki, C., 2022, Trace elements in olivine fingerprint the source of 2018 magmas and shed light on explosive-effusive eruption cycles at Kīlauea Volcano: Earth and Planetary Science Letters, 595 v. doi:10.1016/j.epsl.2022.117769.
Mourey, A.J., Shea, T., Hammer, J.E., 2023. Preservation of magma recharge signatures in kīlauea olivine during protracted storage. J. Geophys. Res. 128, e2022JB025523 https://doi.org/10.1029/2022JB025523.
Nadeau, P.A., Diefenbach, A.K., Hurwitz, S., Swanson, D.A., 2020. From Lava to Water: A New Era at Kīlauea: Eos 101. doi:10.1029/2020EO149557.
Neal, C.A., et al., 2019. The 2018 rift eruption and summit collapse of Kīlauea Volcano. Science 363, 367–374. https://doi.org/10.1126/science.aav7046.
Peltier, A., Poland, M.P., Staudacher, T., 2015. Are Piton de la Fournaise (La Réunion) and Kīlauea (Hawai'i) Really "Analog Volcanoes"?, in Hawaiian volcanoes. AGU 507–531. https://doi.org/10.1002/9781118872079.ch23.
Poland, M.P., Miklius, A., and Montgomery-Brown, E.K., 2014, Magma supply, storage, and transport at shield-stage Hawaiian volcanoes, in Poland, M.P., Takahashi, T.J., and Landowski, C.M. eds., Characteristics of Hawaiian Volcanoes, U.S. Geological Survey Professional Paper 1801, v. 1801, p. 179–234, doi:10.3133/pp18015.
Portnyagin, M., Almeev, R., Matveev, S., Holtz, F., 2008. Experimental evidence for rapid water exchange between melt inclusions in olivine and host magma. earth and Planetary Science Letters 272, 541–552. https://doi.org/10.1016/j.epsl.2008.05.020.
Rasmussen, D.J., Kyle, P.R., Wallace, P.J., Sims, K.W.W., Gaetani, G.A., Phillips, E.H., 2017. Understanding degassing and transport of CO_2-rich alkalic magmas at ross island, antarctica using olivine-hosted melt inclusions. J. Petrol. 58, 841–861. https://doi.org/10.1093/petrology/egx036.
Roedder, E., 1965. Liquid CO_2 inclusions in olivine-bearing nodules and phenocrysts from basalts. Am. Mineral 50, 1746–1782.
Roedder, E., 1984. Fluid inclusions: Reviews in Mineralogy, 12. Mineralogical Society of America, p. 646. https://doi.org/10.1515/9781501508271.
Schmith, J., Swanson, D.A., 2023. Complex styles of phreatomagmatic explosions at Kīlauea Volcano, Hawaii, controlled by magma structure. Frontiers in Earth Science, v 11. doi:10.3389/feart.2023.1153288.
Simonov, V.A., Dobretsov, N.L., Kotlyarov, A.V., Karmanov, N.S., Borovikov, A.A., 2021. Features of mineral crystallization at different stages of the magmatism evolution of the gorely volcano (Kamchatka): data on melt and fluid inclusions. Russ. Geol. Geophys. 62, 83–108. https://doi.org/10.2113/RGG20194100.
Soule, S.A., 2015. Chapter 21 - mid-ocean ridge volcanism. In: Sigurdsson, H. (Ed.), The Encyclopedia of Volcanoes (Second Edition). Academic Press, Amsterdam, pp. 395–403. https://doi.org/10.1016/B978-0-12-385938-9.00021-3.
Steele-MacInnis, M., Esposito, R., Bodnar, R.J., 2011. Thermodynamic model for the effect of post-entrapment crystallization on the H_2O–CO_2 systematics of vapor-saturated, silicate melt inclusions. J. Petrol. 52, 2461–2482. https://doi.org/10.1093/petrology/egr052, v..
Steele-MacInnis, M., Esposito, R., Moore, L.R., Hartley, M.E., 2017. Heterogeneously entrapped, vapor-rich melt inclusions record pre-eruptive magmatic volatile contents. Contrib. Mineral. Petrol. 172, 18. https://doi.org/10.1007/s00410-017-1343-3.
Sterner, S.M., Pitzer, K.S., 1994. An equation of state for carbon dioxide valid from zero to extreme pressures. Contrib. Mineral. Petrol. 117, 362–374. https://doi.org/10.1007/BF00307271.
Sutton, A.J., and Elias, T., 2014, One Hundred Volatile Years of Volcanic Gas Studies at the Hawaiian Volcano Observatory, in Poland, M.P., Takahashi, T.J., and Landowski, C.M. eds., Characteristics of Hawaiian Volcanoes, U.S. Geological Survey Professional Paper 1801, U.S. Geological Survey Professional Paper, v. 1801, p. 179–234, doi:10.3133/pp18017.
Swanson, D.A., and Houghton, B.F., 2019, Products, processes, and implications of Keanakāko'i volcanism, Kīlauea Volcano, Hawai'i, in Poland, M.P., Garcia, M.O., Camp, V.E., and Grunder, A. eds., Field Volcanology: A Tribute to the Distinguished Career of Don Swanson, Geological Society of America, v. 538, doi:10.1130/2018.2538(07).
Swanson, D.A., Rose, T.R., Fiske, R.S., McGeehin, J.P., 2012. Keanakāko'i Tephra produced by 300 years of explosive eruptions following collapse of Kīlauea's caldera in about 1500CE. J. Volcanol. Geotherm. Res. 215–216, 8–25. https://doi.org/10.1016/j.jvolgeores.2011.11.009.
Swanson, D.A., Rose, T.R., Mucek, A.E., Garcia, M.O., Fiske, R.S., Mastin, L.G., 2014. Cycles of explosive and effusive eruptions at Kīlauea Volcano, Hawai'i. Geology 42, 631–634. https://doi.org/10.1130/G35701.1, v..
Thornber, C.R., Orr, T.R., Heliker, C., Hoblitt, R.P., 2015. Petrologic testament to changes in shallow magma storage and transport during 30+ years of recharge and eruption at Kīlauea Volcano, Hawai'i. In: AGU Geophysical Monograph Series, 208, pp. 147–188. https://doi.org/10.1002/9781118872079.ch8.
Tuohy, R.M., Wallace, P.J., Loewen, M.W., Swanson, D.A., Kent, A.J., 2016. Magma transport and olivine crystallization depths in Kīlauea's east rift zone inferred from experimentally rehomogenized melt inclusions. Geochim. Cosmochim. Acta 185, 232–250. https://doi.org/10.1016/j.gca.2016.04.020, v..
Wallace, P.J., Kamenetsky, V.S., Cervantes, P., 2015. Melt inclusion CO_2 contents, pressures of olivine crystallization, and the problem of shrinkage bubbles. Am. Mineral. 100, 787–794. https://doi.org/10.2138/am-2015-5029, v..
Werner, C., et al., 2019. Carbon dioxide emissions from subaerial volcanic regions: two decades in review. In: Orcutt, B.N., Daniel, I., Dasgupta, R. (Eds.), Deep Carbon: Past to Present. Cambridge University Press, Cambridge, pp. 188–236. https://doi.org/10.1017/9781108677950.
Wieser, P.E., Jenner, F.E., Edmonds, M., Maclennan, J., Kunz, B.E., 2020. Chalcophile elements track the fate of sulfur at Kīlauea Volcano, Hawai'i. Geochim. Cosmochim. Acta 282, 245–275. https://doi.org/10.1016/j.gca.2020.05.018.
Wieser, P.E., et al., 2021. Reconstructing magma storage depths for the 2018 kīlauean eruption from melt inclusion CO_2 contents: the importance of vapor bubbles. Geochem. Geophys. Geosyst. 22, e2020GC009364 https://doi.org/10.1029/2020GC009364.
Wieser, P.E., Edmonds, M., Gansecki, C., Maclennan, J., Jenner, F.E., Kunz, B., Antoshechkina, P., Trusdell, F., Lee, R.L., EIMF, 2022. Explosive activity on Kīlauea's lower east rift zone fueled by a volatile-rich. In: Dacitic Melt: Geochemistry, Geophysics, Geosystems, 23, e2021GC010046. https://doi.org/10.1029/2021GC010046.
Wright, T.L., Helz, R.T., 1996. Differentiation and magma mixing on Kilauea's east rift zone: a further look at the eruptions of 1955 and 1960. Part II. The 1960 lavas. bulletin of Volcanology 57, 602–630. https://doi.org/10.1007/s004450050115.
Wright, T.L., Klein, F.W. (Eds.), 2014. Two Hundred Years of Magma Transport and Storage At Kīlauea Volcano, Hawai'i, 1790-2008. US Geological Survey Professional Paper, p. 228. https://doi.org/10.3133/pp1806, 1806.
Zanon, V., Frezzotti, M.L., 2013. Magma storage and ascent conditions beneath Pico and Faial islands (Azores archipelago): a study on fluid inclusions. Geochem. Geophys. Geosyst. 14, 3494–3514. https://doi.org/10.1002/ggge.20221.